Robust Entanglement Gates for Trapped-Ion Qubits

Yotam Shapira,* Ravid Shaniv, Tom Manovitz, Nitzan Akerman, and Roee Ozeri
Department of Physics of Complex Systems, Weizmann Institute of Science, Rehovot 7610001, Israel

(Received 22 May 2018; published 1 November 2018)

High-fidelity two-qubit entangling gates play an important role in many quantum information processing tasks and are a necessary building block for constructing a universal quantum computer. Such high-fidelity gates have been demonstrated on trapped-ion qubits; however, control errors and noise in gate parameters may still lead to reduced fidelity. Here we propose and demonstrate a general family of two-qubit entangling gates which are robust to different sources of noise and control errors. These gates generalize the renowned Mølmer-Sørensen gate by using multitone drives. We experimentally implemented several of the proposed gates on $^{88}Sr^{+}$ ions trapped in a linear Paul trap and verified their resilience.

DOI: 10.1103/PhysRevLett.121.180502

Quantum information processing (QIP) is a rapidly growing field. Two-qubit entanglement gates play an essential part in many QIP tasks, and in particular serve as part of a universal gate set [1,2]. Moreover, the ability to execute high-fidelity gates is necessary in order to achieve fault-tolerant quantum computing [3]. To this end, gates which are less sensitive to control errors would be beneficial.

Trapped ions are a promising platform for QIP applications; therefore, implementing high-fidelity two-qubit entangling gates in trapped-ion systems has been at the center of many experimental investigations [4–10]. In most of these demonstrations, however, fine-tuning and stability of gate parameters were required.

Here we present a general scheme for engineering robust entanglement gates in trapped-ion systems. We generalize the well-known Mølmer-Sørensen (MS) gate [11,12] by using additional frequency components in the laser drive. We show that these components may be used as additional degrees of freedom (d.o.f.) to optimize gate robustness to different noise processes and control errors. Our main results are entangling gates that are robust to gate timing errors, harmonic trap frequency uncertainties, and off-resonance couplings to neighboring transitions.

Recently, several gates with increased resilience to different noises were proposed [13,14] and demonstrated [15–18]. In these, a specific source of infidelity is mitigated by solving, typically numerically, a minimization problem. We provide a general recipe in which one may combine several infidelity sources of choice and determine to what degree each will be treated. The corresponding gate scheme is then given analytically and is straightforward to implement.

We experimentally demonstrate our gates on a $^{88}Sr^{+}$, two-ion crystal, trapped in a linear Paul trap. We define the states $|S\rangle \equiv 5S_{\frac{1}{2},-\frac{1}{2}}$ and $|D\rangle \equiv 4D_{\frac{5}{2},-\frac{3}{2}}$ as our qubit levels. The $|S\rangle \leftrightarrow |D\rangle$ optical quadrupole transition at 674 nm is driven by a narrow-linewidth (< 20 Hz) laser. We cool the ion crystal normal mode to an average phonon number $\bar{n} \approx 0.17$, although some of our data were taken in a Doppler cooled regime with $\bar{n} \approx 9.8$ for comparison. More details about our system can be found in Refs. [19,20].

The MS entangling gate is implemented by driving the qubit transition in a two-ion crystal with a bichromatic field containing the frequencies $\omega_{\pm} = \omega_0 \pm (\nu + \xi_0)$. ω_0 is the resonance frequency of the qubit transition, ν is the frequency of a selected normal mode of the crystal, and ξ_0 is a frequency detuning from the sideband transition. Following Ref. [12], the effective interaction Hamiltonian is $\hat{H} = -2\hbar\eta\Omega\hat{J}_y(\hat{a}e^{i\xi_0 t} + \text{H.c.})$, where $\hat{a}$ is the mode-lowering operator, η is the Lamb-Dicke parameter, Ω is the laser's Rabi frequency, and $\hat{J}_y = (\mathbb{I} \otimes \hat{\sigma}_y + \hat{\sigma}_y \otimes \mathbb{I})/2$ is a global $\hat{y}$ rotation operator in the two-qubit subspace. This interaction yields the unitary evolution operator

$$\hat{U}(t;0) = e^{-iA(t)\hat{J}_y^2} e^{-iF(t)\hat{J}_y\hat{x}} e^{-iG(t)\hat{J}_y\hat{p}}, \tag{1}$$

with

$$\begin{aligned} G(t) &= \frac{\sqrt{2}\eta\Omega}{\xi_0}[1 - \cos(\xi_0 t)], \\ F(t) &= -\frac{\sqrt{2}\eta\Omega}{\xi_0}[\sin(\xi_0 t)], \\ A(t) &= -\int_0^t d\tau F(\tau)\partial_\tau G(\tau). \end{aligned} \tag{2}$$

Equation (1) implies that the ions' evolution follows a trajectory $(G(t), F(t))$ in the normal mode's phase space, which depends on the eigenvalue of $\hat{J}_y$. In the $\hat{J}_y$ basis it acquires a geometric phase $A(t)$, which corresponds to a correlated rotation by an angle equal to the area enclosed by the trajectory. By choosing $\xi_0 = 2\eta\Omega$, the phase-space

trajectory closes at the gate time, defined by $T \equiv 2\pi/\xi_0$ such that $A(T) = \pi/2$.

Ideally, the MS gate generates deterministic, temperature-independent, two-qubit entanglement. However, this requires exact calibration and short-term stability of the gate parameters, such as the gate time T and the normal-mode frequency ν. Inaccuracies and drifts will result in a reduced, temperature-dependent gate fidelity. Furthermore, the MS scheme is substantially slower than the normal-mode period in order to avoid unwanted off-resonance carrier coupling.

To mitigate these shortcomings, we generalize this entangling scheme by employing additional frequency tones. The amplitudes of these tones are then treated as additional d.o.f. and used to reduce, and in some cases eliminate, the effect of errors in different gate parameters on its fidelity, leading to robust entanglement. Here we demonstrate robustness to gate timing errors, normal-mode frequency errors, and the reduction of off-resonance carrier coupling.

Our generalized entangling gate is formally implemented by driving the ions with a multichromatic beam containing N frequency pairs, $\omega_{\pm,i} = \omega_0 \pm (\nu + n_i\xi_0)$, with relative amplitudes r_i and phases satisfying $\phi_{+,i} + \phi_{-,i} = 0$, such that $i = 1, \ldots, N$. We interpret $r_i > 0\,(< 0)$ as $\phi_{+,i} - \phi_{-,i} = 0\,(= \pi)$.

We now turn to deriving the generalized gate Hamiltonian. We assume the ions are well within the Lamb-Dicke regime and expand the interaction Hamiltonian in orders of η to obtain

$$\hat{H} = 2\hbar\Omega\hat{J}_x e^{i\nu t} - 2\hbar\eta\Omega\hat{J}_y \sum_{i=1}^{N} (\hat{a}e^{i\xi_0 n_i t} + \text{H.c.}) \quad (3)$$

The first term in Eq. (3) generates unwanted off-resonance carrier coupling, i.e., local qubit excitations, without involving the normal mode. By assuming that $\Omega \ll \nu$, this term may be neglected in a rotating wave approximation. Since the commutation relations of any of the remaining terms in Eq. (3) are proportional to identity, the Hamiltonian can be solved exactly. The resulting unitary operator is given by the same expression as in Eq. (1); however, with a generalized trajectory given by

$$G(t) = \frac{\sqrt{2}\eta\Omega}{\xi_0} \sum_{i=1}^{N} \frac{r_i}{n_i} [1 - \cos(n_i\xi_0 t)],$$
$$F(t) = -\frac{\sqrt{2}\eta\Omega}{\xi_0} \sum_{i=1}^{N} \frac{r_i}{n_i} [\sin(n_i\xi_0 t)]. \quad (4)$$

Once again, the normal-mode motion follows a trajectory $(G(t), F(t))$ in phase space, accompanied by a correlated rotation in the two-qubit subspace by an angle corresponding to the area enclosed by the trajectory.

Similarly to the MS case, we demand that at the gate time $G(T) = F(T) = 0$ and $A(T) = \pi/2$, which is satisfied by setting

$$n_i \in \mathbb{Z}, \qquad \sum_{i=1}^{N} \frac{r_i^2}{n_i} = 1, \qquad \xi_0 = 2\eta\Omega = \frac{2\pi}{T}. \quad (5)$$

Equation (5) defines a family of entangling gates that differ by the harmonic tones used, $\{n_i\}_{i=1}^N$, and their relative amplitudes, $\{r_i\}_{i=1}^N$. These parameters can be used as additional d.o.f. for optimizing the entangling gate's robustness to different noises or control errors. The case $N = 1$, $n_1 = r_1 = 1$ retrieves the MS entangling gate.

A key component in the optimization is the gate fidelity, $F_g \equiv \langle\psi_{\text{ideal}}|\hat{\rho}(T)|\psi_{\text{ideal}}\rangle$, where ψ_{ideal} is the ideal two-qubit final state and $\hat{\rho}(t)$ is the two-qubit density matrix during the gate evolution. Here, $\hat{\rho}$ is obtained by tracing out the normal-mode d.o.f., yielding

$$F_g = \frac{3 + e^{-4(\bar{n}+\frac{1}{2})\frac{F^2+G^2}{2}}}{8} + \frac{e^{-(\bar{n}+\frac{1}{2})\frac{F^2+G^2}{2}} \sin\left(A + \frac{FG}{2}\right)}{2}, \quad (6)$$

where $\bar{n}$ is the average phonon number assuming an initial thermal state. F_g depends on various physical parameters such as ξ_0, ν, and T. The closed form of Eq. (6) allows for the expansion of F_g in any parameter of choice, α, which may deviate from its ideal value α_0 in the experiment due to imperfections:

$$F_g(\delta\alpha) = 1 + \frac{\partial^2(F_g^2)}{\alpha^2}\bigg|_{\alpha_0} (\delta\alpha)^2 + \mathcal{O}(\delta\alpha^4). \quad (7)$$

Increasing robustness to deviations in α is possible if the leading-order contribution to the fidelity may be minimized or even eliminated by a specific choice of $\{n_i\}$ and $\{r_i\}$.

The first optimization procedure we demonstrate is that of gate timing errors. We set $T = T_0 + \delta T$ and expand the fidelity function. Eliminating the first $N - 1$ leading orders in δT reduces to a set of constraints $V_{\boldsymbol{n}}\boldsymbol{r} = \boldsymbol{0}$, where $\boldsymbol{r}$ is a vector of N amplitudes and $V_{\boldsymbol{n}}$ is an $N \times N$ Vandermonde matrix defined by $(V_{\boldsymbol{n}})_{i,j} = (n_j)^{i-1}$. There are no constraints on the n_i's. Satisfying these leads to a fidelity of the form $1 - F_g \sim (\delta T/T)^{2N}$. For $N = 2$, i.e., eliminating the second-order term, our solution yields $r_1 = -r_2$.

By choosing $n_1 = 1$ and $n_2 = 2$, we obtain an entangling gate with a cardioid (heart-shaped) phase-space trajectory. Inspired by this, we denote all entangling gates which satisfy this set of constraints as *cardioid gates*. Specifically, the heart-shaped gate is a Cardioid(1,2). However, implementing a Cardioid(1,2) may result in unwanted on-resonance sideband excitations due to nonlinear responses of system components (see the Supplemental Material [21]). We mitigate such effects by choosing $n_i \in \{2, 3, 7, 8, \ldots, 5n + 2, 5n + 3\}$.

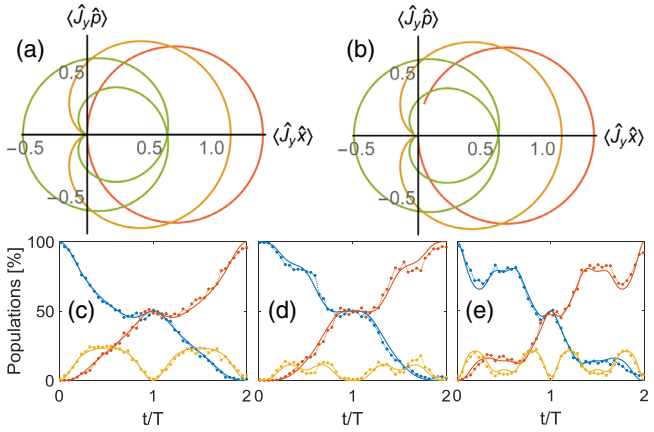

FIG. 1. Phase-space trajectories and population evolution. (a) Phase-space trajectories of MS (red) and the heart-shaped Cardioid(1,2) (orange) and Cardioid(2,3) (green) gates in the absence of errors. All three gates start and end at (0,0) and enclose an area of $\pi/2$. (b) Same as (a), but with a 6% gate timing error. The MS gate no longer closes the trajectory, while the cardioid gates are almost unaffected. (c) Evolution of the MS gate. In this and the following figures, population data (connected circles) of the SS (blue), DD (red) and SD + DS (orange) states are obtained by averaging over 625 realizations, yielding at most 2% projection error, and are compared to the analytic solution (solid line) with no fitting parameters. The gate time, $t = T$, is seen as the SS and DD populations are at 50%, while the SD + DS population vanishes. (d) Cardioid(2,3) gate showing a flat response of the populations around the gate time, indicating increased robustness to timing errors. (e) Antioid(2,3) gate employing the same tones and power as in the Cardioid(2,3) gate, however with uniform phase. We observe a narrow quadratic response around the gate time.

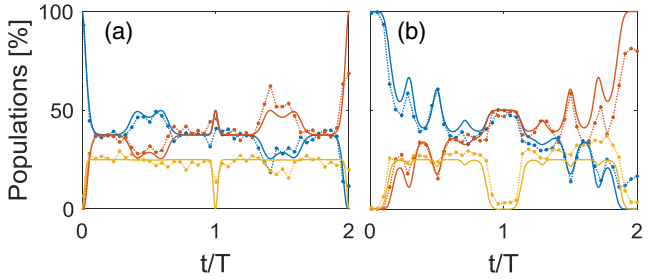

FIG. 2. Finite-temperature gates. Here ions are Doppler cooled to $\bar{n} \approx 9.8$. Color coding is identical to that of Fig. 1(c). (a) Antioid(2,3) gate population evolution. A narrow change around $t = T$ marks ion entanglement. Gate fidelity is very sensitive to timing errors. (b) Cardioid(2,3,7,8) gate population evolution. Using four tones increases the robustness, resulting in a wide feature around gate time.

The reduction of gate error in cardioid gates is the result of coherent interference of the contributions from the different tones. To show this, we compare the cardioid with an entangling gate which uses the same tones and amplitudes, but with all amplitudes having the same phase. The resulting gate has an increased sensitivity to gate timing errors. Since this gate has the opposite effect on timing-error robustness, we refer to this family of gates as *antioid gates*.

An intuitive understanding of the origin of robustness to timing errors can be gained by observing that the cardioid constraint is simply a demand for order-N smoothness of F and G at the beginning and end of the gate. This means that the spin-dependent forces applied by the gate vary smoothly towards the gate's beginning and end as well.

Figures 1(a) and 1(b) show a comparison between the phase-space trajectory formed by the MS (red), Cardioid (1,2) (orange), and Cardioid(2,3) (green) gates for an ideal scenario and in the presence of a 6% gate timing error. Robustness is evident, as the cardioid trajectories seem almost unaffected by the error. Furthermore, the cardioid gates' trajectories remain closer to the origin, indicating that less motion of the ion crystal is excited. Figures 1(c)–1(e) show the measured and analytically calculated evolution of the qubit-state population for the MS, Cardioid(2,3), and Antioid(2,3) gates, respectively. Compared to the standard MS gate, the Cardioid(2,3) shows a variation of the ion-state populations around the gate time which is flatter than quadratic, while the Antioid(2,3) has a faster quadratic response.

Due to the dependence of the fidelity on $\bar{n}$ in Eq. (6), any small deviation of $F(T)$ or $G(T)$ from 0 will result in errors that are exponentially amplified by $\bar{n}$. Therefore, robustness is especially important when implementing entangling gates in systems which are not cooled to the normal-mode ground state. Figure 2 shows the population evolution of antioid and cardioid gates and their corresponding robustness to timing errors in a Doppler cooled regime, with $\bar{n} \approx 9.8$. As seen, the antioid gate is highly sensitive to gate timing errors at this high temperature, whereas the cardioid gate shows a flatter response.

We next turn to optimizing our gate to mitigate off-resonance carrier coupling. The gate error due to this effect is given by [12]

$$1 - F_d = \sum_{n=0}^{\infty} \frac{(-1)^n}{(2n)!} \left(\frac{2\Omega \sin(\nu T)}{\nu} \sum_{i=1}^{N} \frac{r_i}{1 - \frac{2n_i \eta \Omega}{\nu}} \right)^{2n}. \quad (8)$$

Interestingly, eliminating this term in increasing orders of Ω/ν yields exactly the cardioid set of constraints, indicating that the cardioid gate will eliminate both timing as well as carrier coupling errors. As an example, a typical MS gate with $\Omega_0/\nu = 0.1$ and gate time T_0 suffers from ~2% infidelity due to off-resonance carrier coupling. Increasing the Rabi frequency to $3\Omega_0$ will result in a gate time $\frac{1}{3}T_0$ but also increases the infidelity by an order of magnitude. However, using a Cardioid(1,2) gate with a $3\Omega_0$ Rabi frequency will result in ~0.1% infidelity with a gate time $\sqrt{\frac{8}{9}}T_0 \approx 0.55T_0$. Figure 3 shows the effect of off-resonance coupling on the MS and Cardioid(2,3) gates. As seen in the

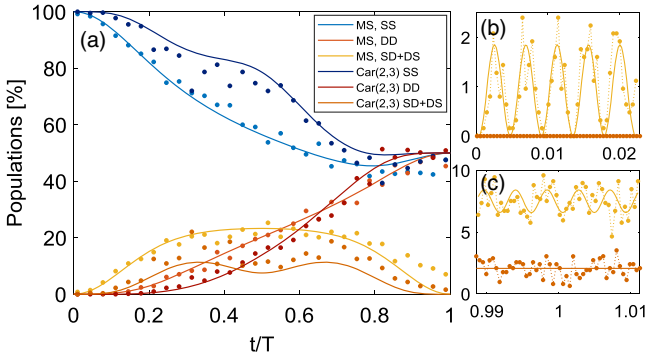

FIG. 3. Off-resonance carrier coupling. (a) Population evolution of the MS and Cardioid(2,3) gates, showing data (circles) and analytical solution (solid lines). Here $\Omega/\nu \sim 5\%$, which, according to Eq. (8), corresponds to 2% infidelity for the MS gate and 0.1% for the Cardioid(2,3) gate. This infidelity is seen by the SD + DS populations not vanishing at the gate time. (b) Zoom-in scan of SD + DS populations at the gate start. Fast carrier oscillations are easily observed for the MS gate (yellow points). These are heuristically fitted to off-resonance Rabi oscillations $A\sin^2(\sqrt{\Omega^2+\nu^2}t)$ (yellow line). For the cardioid no such oscillations are seen. (c) Zoom-in scan of SD + DS populations around the gate time. The carrier oscillations are less distinct, since here projection noise is on par with the oscillation amplitude. The MS gate populations oscillate around 8% at gate time, while the cardioid populations oscillate around 2%, which corresponds directly to an increased gate fidelity. The 2% cardioid infidelity is due to other imperfections and not carrier coupling.

MS gate, fast oscillations of SD + DS populations are caused by off-resonance carrier coupling. These are significantly suppressed in the cardioid gate.

Intuitively, this works since a smoother gate envelope has a narrower spectral content and therefore less overlap with off-resonance transitions such as the carrier. Using smooth gate envelopes to reduce carrier coupling has already been suggested [22] and implemented [5]. Here we have provided a general treatment that does not rely on spectral density arguments and does not require intermediate additional pulses as proposed in Ref. [22], which compensate for a spectral overlap with the motional sideband transitions.

We turn to optimize the gate to mitigate normal-mode frequency errors. In many implementations this parameter is actively stabilized to avoid errors [10,23]. Here, we set $\nu = \nu_0 + \delta\nu$ and employ our optimization procedure. This yields a set of constraints $V_{\boldsymbol{n}^{-1}}\boldsymbol{r} = \boldsymbol{0}$, where this time the Vandermonde matrix is $(V_{\boldsymbol{n}^{-1}})_{i,j} = (n_j)^{-i}$. As opposed to timing-error robustness, the quadratic term cannot be eliminated, and the fidelity always scales quadratically in $\delta\nu/\xi_0$. However, the prefactor of this quadratic term is minimized. The gate purity, which is a measure of disentanglement from the motion, defined as $P_g \equiv \mathrm{Tr}(\hat{\rho}^2)$, does become robust order by order. This is important, since it

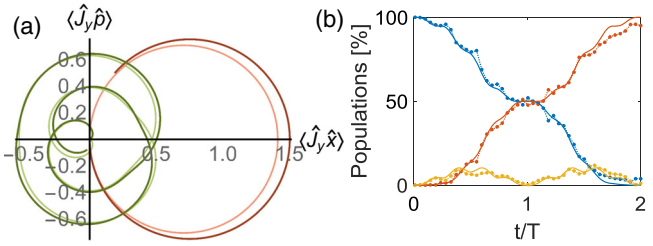

FIG. 4. CarNu(2,3,7) gate. (a) Phase-space trajectory of MS (red) and CarNu(2,3,7) (green) gates for an ideal case (light) and for a combined 6% timing error and 6% normal-mode frequency error (dark). Clearly, the CarNu(2,3,7) gate displays robustness, as its trajectory is almost unaffected. (b) Population evolution of CarNu(2,3,7). Color coding is the same as in Fig. 1(c). The plot shows a flat response of the state populations around the gate time, indicating increased robustness to timing errors.

reduces the number of error syndromes that need to be considered when implementing quantum error correction. This quadratic scaling of the fidelity encourages us to add only one d.o.f., as minimizing higher orders will have a marginal effect. However, adding further tones may be used to combine this with eliminating timing errors and off-resonance carrier coupling. We denote this type of combined entangling gate as a *CarNu gate*. Figure 4 shows the phase-space trajectory and population evolution of the CarNu(2,3,7) gate, which demonstrates robustness to gate timing errors and off-resonance carrier coupling, as well as normal-mode frequency errors.

Finally, we directly measure the fidelity of the different gates and observe their robustness properties. Figure 5(a) shows the fidelity of the different gates as a function of gate timing error. Cardioid gates display increased robustness,

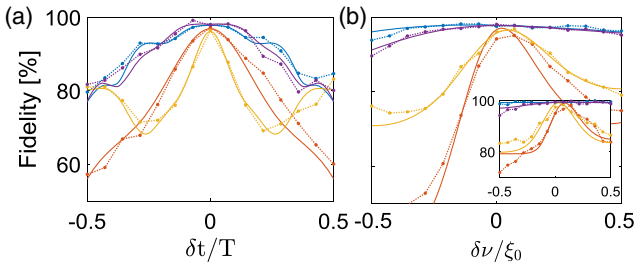

FIG. 5. Gate fidelities, showing data (filled circles) and a rescaled analytical solution (solid lines). (a) Gate fidelity vs timing error. The MS (red) and Antioid(2,3) (orange) fidelities scale quadratically with the timing error, with the antioid showing the narrowest response. The CarNu(2,3,7) (blue) and Cardioid (2,3,7) (purple) fidelities have fourth- and sixth-order dependences on the timing error, respectively, and are therefore more resilient. (b) Gate fidelity vs normal-mode frequency errors. Here optimization is not order by order; rather, the prefactor of the quadratic term is minimized. The CarNu(2,3,7) (blue) shows the flattest response compared to the other entangling schemes. The inset shows gate purity, for which the optimization is order by order. The CarNu(2,3,7) purity has a fourth-order dependence on the error, while the other gates scale quadratically.

seen as a higher-order flat response to timing errors. Figure 5(b) shows the fidelity of the different gates as a function of normal-mode frequency error. As expected, the CarNu gate displays the flattest response. Our robust entangling gates also display a slightly increased maximal fidelity; however, this is not a substantial improvement on our typical gate fidelity, showing that our gates are limited by other factors. We estimate that the dominant of those is fast phase noise, at 0.5–1.5 MHz, in our narrow-linewidth laser, which incoherently couples to the carrier transition during the gate drive.

We state, without demonstration, that the CarNu(2,3,7) gate also mitigates errors due to normal-mode heating [18] and errors due to motional coupling to neighboring normal modes (see the Supplemental Material [21]).

In conclusion, we have analytically derived and experimentally demonstrated a scheme for robust entanglement gates for trapped-ion qubits. Our scheme increases the robustness to gate timing errors and normal-mode frequency errors as well as reducing off-resonance carrier coupling. This allows for the use of higher laser power and the implementation of faster entangling gates while maintaining high gate fidelities. This optimization is particularly important when working with larger Coulomb crystals where the spectral distance between modes is small. From a broader point of view, we believe our methodology offers a simple and straightforward prescription for increasing the efficiency of entangling operations, which are an essential tool in quantum information experiments, as well as many other research directions.

This work was supported by the Crown Photonics Center, the ICore-Israeli Excellence Center Circle of Light, the Israeli Science Foundation, the Israeli Ministry of Science Technology and Space, the Minerva Stiftung, and the European Research Council (consolidator Grant No. 616919-Ionology).

Note added.—Recently, we have become aware of related work, based on Ref. [13], where RF entanglement gates were made more resilient to normal-mode heating and frequency drifts [18].

*yotam.shapira@weizmann.ac.il

[1] A. Barenco, C. H. Bennett, R. Cleve, D. P. DiVincenzo, N. Margolus, P. Shor, T. Sleator, J. A. Smolin, and H. Weinfurter, Elementary gates for quantum computation, Phys. Rev. A **52**, 3457 (1995).

[2] A. Y. Kitaev, Quantum computations: algorithms and error correction, Russ. Math. Surv. **52**, 1191 (1997).

[3] D. Aharonov and M. Ben-Or, Fault-tolerant quantum computation with constant error rate, SIAM J. Comput. **38**, 1207 (2008).

[4] D. Leibfried, B. DeMarco, V. Meyer, D. Lucas, M. Barrett, J. Britton, W. M. Itano, B. Jelenkovic, C. Langer, T. Rosenband, and D. J. Wineland, Experimental demonstration of a robust, high-fidelity geometric two ion-qubit phase gate, Nature (London) **422**, 412 (2003).

[5] G. Kirchmair, J. Benhelm, F. Zähringer, R. Gerritsma, C. F. Roos, and R. Blatt, Deterministic entanglement of ions in thermal states of motion, New J. Phys. **11**, 023002 (2009).

[6] J. P. Gaebler, T. R. Tan, Y. Lin, Y. Wan, R. Bowler, A. C. Keith, S. Glancy, K. Coakley, E. Knill, D. Leibfried, and D. J. Wineland, High-Fidelity Universal Gate Set for $^{9}Be^{+}$ Ion Qubits, Phys. Rev. Lett. **117**, 060505 (2016).

[7] C. J. Ballance, T. P. Harty, N. M. Linke, M. A. Sepiol, and D. M. Lucas, High-Fidelity Quantum Logic Gates Using Trapped-Ion Hyperfine Qubits, Phys. Rev. Lett. **117**, 060504 (2016).

[8] T. P. Harty, M. A. Sepiol, D. T. C. Allcock, C. J. Ballance, J. E. Tarlton, and D. M. Lucas, High-Fidelity Trapped-Ion Quantum Logic Using Near-Field Microwaves, Phys. Rev. Lett. **117**, 140501 (2016).

[9] S. Weidt, J. Randall, S. C. Webster, K. Lake, A. E. Webb, I. Cohen, T. Navickas, B. Lekitsch, A. Retzker, and W. K. Hensinger, Trapped-Ion Quantum Logic with Global Radiation Fields, Phys. Rev. Lett. **117**, 220501 (2016).

[10] H. Kaufmann, T. Ruster, C. T. Schmiegelow, M. A. Luda, V. Kaushal, J. Schulz, D. von Lindenfels, F. Schmidt-Kaler, and U. G. Poschinger, Scalable Creation of Long-Lived Multipartite Entanglement, Phys. Rev. Lett. **119**, 150503 (2017).

[11] K. Mølmer and A. Sørensen, Multiparticle Entanglement of Hot Trapped Ions, Phys. Rev. Lett. **82**, 1835 (1999).

[12] A. Sørensen and K. Mølmer, Entanglement and quantum computation with ions in thermal motion, Phys. Rev. A **62**, 022311 (2000).

[13] F. Haddadfarshi and F. Mintert, High fidelity quantum gates of trapped ions in the presence of motional heating, New J. Phys. **18**, 123007 (2016).

[14] M. Palmero, S. Martinez-Garaot, D. Leibfried, D. J. Wineland, and J. G. Muga, Fast phase gates with trapped ions, Phys. Rev. A **95**, 022328 (2017).

[15] T. Manovitz, A. Rotem, R. Shaniv, I. Cohen, Y. Shapira, N. Akerman, A. Retzker, and R. Ozeri, Fast Dynamical Decoupling of the Mølmer-Sørensen Entangling Gate, Phys. Rev. Lett. **119**, 220505 (2017).

[16] V. M. Schfer, C. J. Ballance, K. Thirumalai, L. J. Stephenson, T. G. Ballance, A. M. Steane, and D. M. Lucas, Fast quantum logic gates with trapped-ion qubits, Nature (London) **555**, 75 (2018).

[17] P. H. Leung, K. A. Landsman, C. Figgatt, N. M. Linke, C. Monroe, and K. R. Brown, Robust 2-Qubit Gates in a Linear Ion Crystal Using a Frequency-Modulated Driving Force, Phys. Rev. Lett. **120**, 020501 (2018).

[18] A. E. Webb, S. C. Webster, S. Collingbourne, D. Bretaud, A. M. Lawrence, S. Weidt, F. Mintert, and W. K. Hensinger, Resilient Entanglement Gates For Trapped Ions, Phys. Rev. Lett. **121**, 180501 (2018).

[19] N. Akerman, Y. Glickman, S. Kotler, A. Keselman, and R. Ozeri, Quantum control of $^{88}Sr^{+}$ in a miniature linear Paul trap, Appl. Phys. B **107**, 1167 (2012).

[20] N. Akerman, N. Navon, S. Kotler, Y. Glickman, and R. Ozeri, Universal gate-set for trapped-ion qubits using a

narrow linewidth diode laser, New J. Phys. **17**, 113060 (2015).

[21] See Supplemental Material at http://link.aps.org/supplemental/10.1103/PhysRevLett.121.180502 for further details regarding the nonlinear responses in Cardioid(1,2) and mitigation methods.

[22] C. F. Roos, Ion trap quantum gates with amplitude-modulated laser beams, New J. Phys. **10**, 013002 (2008).

[23] K. G. Johnson, J. D. Wong-Campos, A. Restelli, K. A. Landsman, B. Neyenhuis, J. Mizrahi, and C. Monroe, Active stabilization of ion trap radiofrequency potentials, Rev. Sci. Instrum. **87**, 053110 (2016).